


Black-hole horizon in the Dirac semimetal $\text{Zn}_2\text{In}_2\text{S}_5$ Huaqing Huang,¹ Kyung-Hwan Jin,¹ and Feng Liu^{1,2,*}¹*Department of Materials Science and Engineering, University of Utah, Salt Lake City, Utah 84112, USA*²*Collaborative Innovation Center of Quantum Matter, Beijing 100084, China* (Received 17 August 2017; revised manuscript received 8 February 2018; published 26 September 2018)

Recently, realizing new fermions, such as type-I and type-II Dirac/Weyl fermions in condensed matter systems, has attracted considerable attention. Here, we show that the transition state from type-I to type-II Dirac fermions can be viewed as a “type-III” Dirac fermion, which exhibits unique characteristics, including a Dirac-line Fermi surface with a nontrivial topological invariant and critical chiral anomaly effect, distinct from previously known Dirac semimetals. Most importantly, we discover $\text{Zn}_2\text{In}_2\text{S}_5$ is a type-III Dirac semimetal, characterized by a pair of Dirac points in the bulk and Fermi arcs on the surface. We further propose a solid-state realization of the black-hole-horizon analog in inhomogeneous $\text{Zn}_2\text{In}_2\text{S}_5$ to simulate black-hole evaporation with a high Hawking temperature. We envision that our findings will stimulate researchers to study the physics of type-III Dirac fermions, as well as astronomical problems in a condensed matter analog.

DOI: [10.1103/PhysRevB.98.121110](https://doi.org/10.1103/PhysRevB.98.121110)

Introduction. The conception of topology [1–3] has been known in condensed matter physics since the 1980’s. However, it is only recently that we have witnessed an exponential growth in the field of topological phases of matter in the last decade, owing to the introduction of the concept of topological insulators (TIs) [4] and their proposition [5] and confirmation [6] in real material systems. This effective route to discovering TIs from theoretical conception to computational material proposition and to experimental confirmation has been followed by the discovery of other topological materials, such as topological crystalline insulators [7–9], Dirac semimetals [10–13], and most recently Weyl semimetals [14–17]. Depending on the geometry of the Dirac cone, there are type-I and type-II Dirac/Weyl semimetals [18–22]. Interestingly, it has been shown that the interface or the “transition state” from type I to type II has distinctly different topological properties [23–25], which we will call a “type-III” semimetal. Both type-I and type-II Dirac/Weyl semimetals have been experimentally confirmed in real materials [11,13,17,19,21]; however, so far type-III Dirac/Weyl semimetals remain a theoretical conception. Here, we will fill this outstanding gap by proposing a type-III semimetallic phase in $\text{Zn}_2\text{In}_2\text{S}_5$.

Topological semimetals host interesting new types of fermions as low-energy quasiparticles. They not only exhibit novel physical properties such as topological surface states [10–18], a large linear magnetoresistance [26–28], and chiral anomaly [29–34], but also offer a versatile platform for simulating relativistic particles of high-energy physics as well as “new particles” that have no counterparts in high-energy physics. The type-III Dirac semimetal has been theoretically proposed for realizing a solid-state analog of the black-hole horizon [23–25]. To this end, we will again fill the gap by devising a material platform, an inhomogeneous $\text{Zn}_2\text{In}_2\text{S}_5$,

to simulate Hawking radiation at the black-hole horizon. Especially, we suggest a high Hawking temperature associated with the analogous black-hole horizon in $\text{Zn}_2\text{In}_2\text{S}_5$ to ease the experimental observation, in contrast to the low Hawking temperature in previously proposed black-hole-horizon analogs [35–39].

We will first highlight the key features of the type-III Dirac semimetals, including their unique Dirac-line Fermi surface with a nontrivial topological invariant and critical chiral magnetic effect, in distinction from those of type-I and type-II Dirac semimetals. Then we will present evidence that $\text{Zn}_2\text{In}_2\text{S}_5$ is a candidate material for realizing type-III Dirac fermions. Based on an effective Hamiltonian analysis and first-principles calculations, we show the properties of $\text{Zn}_2\text{In}_2\text{S}_5$, including a critical chiral magnetoresistance and Fermi arcs. Finally, we will describe a solid-state realization of the black-hole-horizon analog in inhomogeneous $\text{Zn}_2\text{In}_2\text{S}_5$, to simulate black-hole evaporation with a relatively high Hawking temperature.

The concept of type-III Dirac/Weyl points. Topological Dirac and Weyl semimetals are characterized by fourfold and twofold linear band crossings at the Fermi level (the so-called Dirac and Weyl points), respectively. They can be further classified into two types by fermiology. The type-I Dirac/Weyl semimetals have a typical conical dispersion and a pointlike Fermi surface [Fig. 1(a)] [10–13,16,17]. The type-II Dirac/Weyl semimetals have an overtilted cone-shape band structure, possessing both electron and hole pockets that contact at the type-II Dirac/Weyl point [Fig. 1(b)] [18–22]. The type-III Dirac semimetal is distinct from both type-I and type-II semimetals [41]. (See Table I.) As illustrated in Fig. 1(c), the type-III Dirac point is also a protected band crossing point, but appears at the contact of a linelike Fermi surface. Unlike Fermi surfaces of other topological semimetals, such a unique linelike Fermi surface, the so-called Dirac line, is protected by a topological invariant which is an integer only for the relatively rare Dirac line.

*Corresponding author: fliu@eng.utah.edu

TABLE I. Comparison between three types of Dirac semimetals.

	Type-I	Type-II	Type-III
Dispersion	Dirac cone	Overtilted Dirac cone	Critical Dirac cone
Fermi surface	Pointlike	Electron and hole pockets	Dirac line (with $N_2 = 1$)
DOS (E_F)	Vanishing	Parabolic peak	Finite
Surface Fermi arc	✓	✓	✓
Chiral anomaly	Along all directions	Anisotropic, inside a cone region [40]	Except for the critical plane [41]
Black-hole analog	Outside	Inside	Horizon
Typical materials	Na_3Bi [10], Cd_3As_2 [12]	PtTe_2 [20,21], VAl_3 [22]	$\text{Zn}_2\text{In}_2\text{S}_5$ (this work)

Since a Dirac point can be viewed as the merger of a pair of Weyl points with opposite chirality, we start by considering a general 4×4 Hamiltonian composed of two 2×2 Hamiltonians describing Weyl points for simplicity,

$$H(\mathbf{k}) = \begin{pmatrix} h(\mathbf{k}) & 0 \\ 0 & h^*(-\mathbf{k}) \end{pmatrix}, \quad (1)$$

with

$$h(\mathbf{k}) = \mathbf{v} \cdot \mathbf{k} \sigma_0 + \sum_{i,j} k_i A_{ij} \sigma_j, \quad (2)$$

where σ_j are Pauli matrices and σ_0 is the identity matrix. The energy spectrum of a Weyl point is $E_{\pm}(\mathbf{k}) = \sum_i v_i k_i \pm \sqrt{\sum_j (\sum_i k_i A_{ij})^2} = T(\mathbf{k}) \pm U(\mathbf{k})$. It is well known that if there exists a direction for which $T > U$, the band crossing point is a type-II Dirac point, otherwise it is type I. If and only if for a particular direction \hat{k} that $T(\hat{k}) = U(\hat{k})$, but $T(\hat{k}) < U(\hat{k})$ for other directions, the Dirac points are connected by a linelike Fermi surface as for the type-III Dirac semimetal. It is distinctively different from the type-I pointlike Fermi surface or the type-II hyperbolic Fermi surface (coexistence of electron and hole pockets). The Dirac line is protected by the combination of topology and symmetry, and can be described by a topological invariant [24],

$$N_2 = \frac{1}{4\pi i} \text{Tr} \left[K \oint_c dl h(\mathbf{k})^{-1} \partial_l h(\mathbf{k}) \right], \quad (3)$$

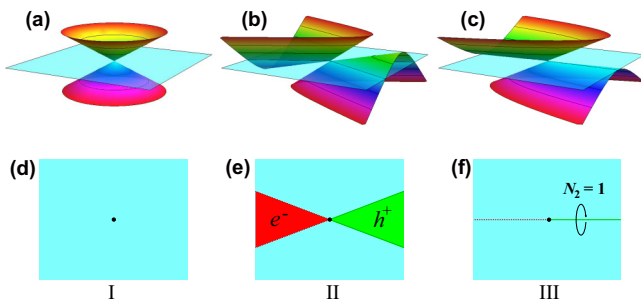


FIG. 1. (a) Type-I Dirac point with a pointlike Fermi surface. (b) The type-II Dirac point is the contact point between the electron and hole pocket. (c) A type-III Dirac point appears as the touching point between Dirac lines. The Dirac line is described by the topological invariant $N_2 = 1$. The light blue semitransparent plane corresponds to the position of the Fermi level, and the black solid/dashed lines mark the boundary of hole/electron pockets. (d)–(f) Fermi surfaces of three types of Dirac semimetals.

where C is a contour enclosing the Dirac line in momentum space. Here, the symmetry operator K depends on the direction of the Dirac line; for the Dirac line along the k_z direction, $K = \sigma_z$ (see Supplemental Material [42]). The topological invariant is actually a winding number of phase around the line, and it stabilizes the Dirac line in the sense that the integral is an integer, $N_2 = 1$ only for a type-III semimetal. The Dirac line with a nonzero winding number is an analog of the vortex line in superfluids [37].

Interestingly, the Dirac cone band structure is tilted exactly with a flatband without dispersion along the particular direction of $E_n(\mathbf{k}) = 0$, which serves as a characteristic feature of type-III Dirac cones. The apparent qualitative distinction between the Fermi surface and band dispersion of type III and those of other types of Dirac cones lead to significant differences in their physical properties, such as a critical chiral magnetoresistance [40]. In particular, the chiral anomaly appears in a type-III Dirac semimetal for almost all the directions of magnetic field. Only when the direction of the magnetic field is exactly perpendicular to the tilt, do the Landau levels collapse due to the open semiclassical cyclotron orbit having no chiral zero mode (see Supplemental Material [42]). We note that also different from type-I and type-II Dirac fermions which exist over a wide range of “phase” space (tilting angle), type III exists only at a fixed tilting angle so that in this sense it is less robust than the types I and II.

Furthermore, the type-III Dirac semimetal can also be viewed as the critical state of Lifshitz transition between types I and II [24]. It was investigated recently as a solid-state realization of a black-hole-horizon analog based on inhomogeneous topological semimetals [23–25]. So far, however, no material system is known to be a type-III Dirac semimetal. Next, we will demonstrate $\text{Zn}_2\text{In}_2\text{S}_5$ to be a type-III Dirac semimetal, and how to realize its black-hole-horizon analog.

The type-III Dirac semimetal state in $\text{Zn}_2\text{In}_2\text{S}_5$. $\text{Zn}_2\text{In}_2\text{S}_5$ has a layered structure consisting of nonuple layers stacked together along the z direction [42]. Each nonuple layer consists of two In and two Zn layers which are sandwiched by S layers alternately, and every In or Zn atom lies in the center of a tetrahedron or octahedron of S atoms. The coupling is strong between atomic layers within the nonuple layer but much weaker between adjacent nonuple layers. By different stackings of these basic building blocks, two kinds of $\text{Zn}_2\text{In}_2\text{S}_5$ arise, i.e., AB-stacked hexagonal structure with $P6_3mc$ symmetry and ABC-stacked rhombohedral structure with $R3m$ symmetry.

We first calculated the band structure of $\text{Zn}_2\text{In}_2\text{S}_5$. As shown in Figs. 2(a) and 2(d), there are flatbands along the

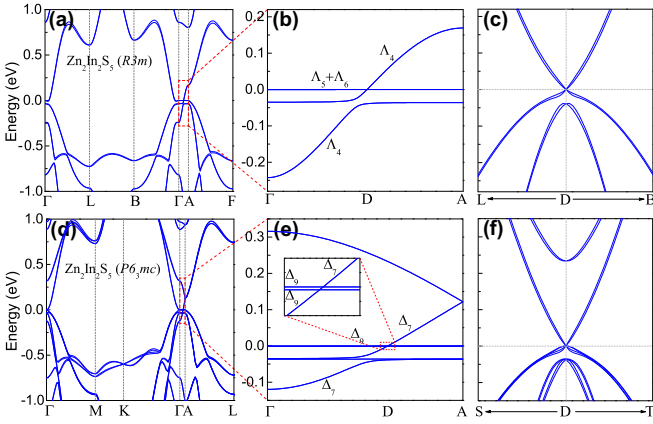


FIG. 2. Band structures of (a)–(c) $\text{Zn}_2\text{In}_2\text{S}_5(R3m)$ and (d)–(f) $\text{Zn}_2\text{In}_2\text{S}_5(P6_3mc)$. (b) and (e) The zoom-in band structures along Γ -A of $\text{Zn}_2\text{In}_2\text{S}_5(R3m)$ and $\text{Zn}_2\text{In}_2\text{S}_5(P6_3mc)$, respectively. (c) and (f) The in-plane band dispersions around the Fermi level of $\text{Zn}_2\text{In}_2\text{S}_5(R3m)$ and $\text{Zn}_2\text{In}_2\text{S}_5(P6_3mc)$, respectively.

Γ -A direction near the Fermi level. Meanwhile, another band disperses upward crossing the flatbands in between Γ and A. The upward dispersive band crosses with the upper flatband but avoids crossing with the lower flatband [Figs. 2(b) and 2(e)]. The band crossings occur in both materials, because the two crossed bands belong to different irreducible representations of the crystal symmetry group. For $\text{Zn}_2\text{In}_2\text{S}_5(R3m)$, the two bands belong to two-dimensional (2D) Λ_4 and one-dimensional (1D) Λ_5/Λ_6 representations, respectively, as distinguished by C_{3v} symmetry around the k_z axis. The different representation prohibits hybridization between them, resulting in a pair of three-dimensional (3D) Dirac points at $\pm(0.254, 0.254, 0.254)$ (in units of $2\pi/a$). For $\text{Zn}_2\text{In}_2\text{S}_5(P6_3mc)$, the upper flatband and the upward dispersive band belong to 2D Δ_9 and Δ_7 , respectively, of the C_{6v} symmetry. One unique feature of the $P6_3mc$ structure is that there are actually adjacent double Dirac points $(0, 0, \pm 0.306)$ and $(0, 0, \pm 0.308)$ [in units of $(2\pi/a, 2\pi/a, 2\pi/c)$] with an energy difference of 1.0 meV. This is because there are actually two flat Δ_9 bands that are close to each other but not exactly degenerate [see the inset of Fig. 2(e)]. Since neither a $R3m$ nor a $P6_3mc$ structure has inversion symmetry, these Dirac semimetals have fourfold degenerate Dirac points, but with splitting of in-plane band dispersions away from the Dirac points [Figs. 2(c) and 2(f)]. This is a unique feature of $\text{Zn}_2\text{In}_2\text{S}_5$, which is different from other Dirac semimetals that require both time-reversal and inversion symmetries. Additionally, we also investigate the strain effect on the electronic structure and found that the position of type-III Dirac points in the k_z axis can be effectively tuned by external strain. As the two structures share similar electronic properties, we take $\text{Zn}_2\text{In}_2\text{S}_5(R3m)$ as an example hereafter.

To further reveal the nature of the type-III Dirac points, we fit first-principles results to a low-energy effective model [42]. Neglecting the insignificant tiny splitting induced by inversion symmetry breaking, the quasiparticles are described by a pair of Weyl Hamiltonians in the vicinity of one Dirac point,

$$h_{\pm}^c = c_{\perp}(k_x\sigma_x \pm k_y\sigma_y) + c_{\parallel}\delta k_z\sigma_z + v\delta k_z\sigma_0, \quad (4)$$

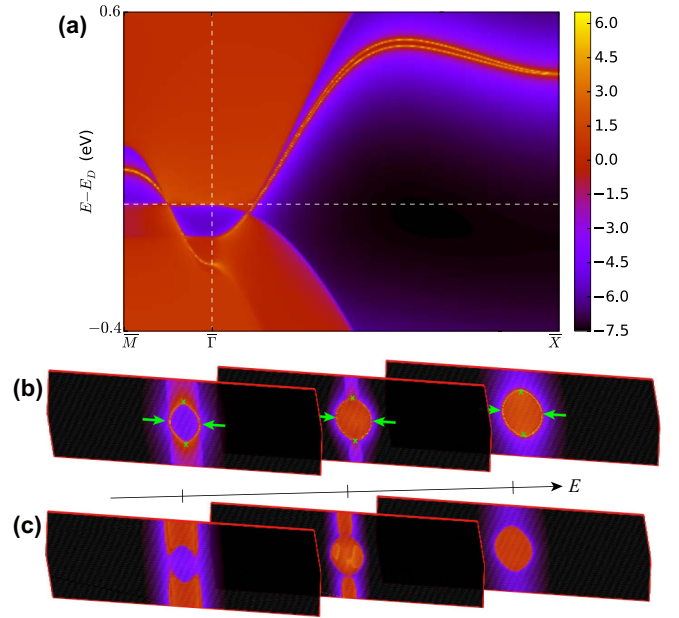


FIG. 3. (a) The projected surface density of states for the (100) surface of $\text{Zn}_2\text{In}_2\text{S}_5(R3m)$ where the nontrivial topological surface states originating from the surface projection of bulk Dirac point are clearly visible. (b) and (c) Constant energy contours of the (100) surface and the bulk at $E = E_F - 25$, E_F and $E_F + 25$ meV, respectively. The green arrows and crosses mark two pieces of Fermi arcs and the surface projection of bulk Dirac points, respectively.

where $\delta k_z = k_z - k_z^c$, with $k_z^c = 0.102 \text{ \AA}^{-1}$. The parameters $c_{\perp} = 2.29$ and $v = -c_{\parallel} = 1.36 \text{ eV \AA}$, indicating that there exists a flatband along \hat{k}_z direction. It is straightforward to derive the topological invariant using $K = \pm\sigma_z$ in Eq. (3) and find that $N_2 = 1$. We thus conclude that $\text{Zn}_2\text{In}_2\text{S}_5$ is a type-III Dirac semimetal.

The topological nature of the type-III Dirac point in $\text{Zn}_2\text{In}_2\text{S}_5$ is also confirmed by calculating the \mathbb{Z}_2 topological invariants which are well defined in the $k_z = 0$ and $k_z = \pi$ planes. For the $k_z = 0$ plane, $\mathbb{Z}_2 = 1$, while for the $k_z = \pi$ plane, $\mathbb{Z}_2 = 0$. Therefore, a band order inversion between Λ_4 and $\Lambda_5 + \Lambda_6$ bands must occur along the k_z direction [see Fig. 2(b)], resulting in a band-gap closure at the Dirac point.

Topological surface states and Fermi arcs are expected to appear on the side surfaces of $\text{Zn}_2\text{In}_2\text{S}_5$. Figure 3 shows the projected surface density of states (DOS) for the (100) surface of a semi-infinite $\text{Zn}_2\text{In}_2\text{S}_5(R3m)$ system. It is seen that the topological surface state emanates from one projection of the bulk Dirac point on the (100) surface, as shown in Fig. 3(a). The Fermi surface contains two pieces of half-circle Fermi arcs, as shown in Fig. 3(b), touching at two singularity points where the surface projections of bulk Dirac points appear. Due to the flat Dirac-line Fermi surface, the shape of the electron and hole pockets varies rapidly with the increasing chemical potential. All these characteristics should be experimentally observable by the modern angle-resolved photoemission spectroscopy technique.

The black-hole-horizon analog. Now we discuss the possibility of realizing a solid-state analog of the black-hole horizon in $\text{Zn}_2\text{In}_2\text{S}_5$. So far, various black-hole analogs have been

proposed [43], such as a sonic black hole for sound waves propagating in flowing liquid [35] and a black-hole/white-hole pair in superfluid He with a moving vierbein domain well [36,37]. In Eq. (4), the last term is the same as the Doppler shift for quasiparticles under a Galilean transformation to a moving frame of reference with a velocity v . In general relativity, a relativistic quasiparticle in (3+1)-dimensional spacetime can be described by the line element $ds^2 = g_{\mu\nu} dx^\mu dx^\nu$, where $g_{\mu\nu}$ is the inverse (covariant) metric describing an effective curved spacetime in which the relativistic quasiparticles propagate [44]. To obtain a spacetime interpretation, we derive an effective covariant metric $g_{\mu\nu}$ according to Eq. (4) [42],

$$g_{\mu\nu} = \begin{pmatrix} -(1 - v^2/c_{\parallel}^2) & 0 & 0 & -v/c_{\parallel}^2 \\ 0 & 1/c_{\perp}^2 & 0 & 0 \\ 0 & 0 & 1/c_{\perp}^2 & 0 \\ -v/c_{\parallel}^2 & 0 & 0 & 1/c_{\parallel}^2 \end{pmatrix}, \quad (5)$$

which has a similar form of the acoustic metric of Unruh's sonic black hole [35,43].

Now let us assume that the dragging velocity $v = v(z)$ depends on the spatial z coordinate in an inhomogeneous $\text{Zn}_2\text{In}_2\text{S}_5$ system, which can, in principle, be realized by a controllable (tunable) structural distortion. As the metric has translation invariance in the x and y directions, for simplicity, we make a dimension reduction to the (1+1)-dimensional spacetime by ignoring the coordinates x and y . As a result, the corresponding linear element becomes

$$ds^2 = -\left(1 - \frac{v^2(z)}{c_{\parallel}^2}\right) d\tau^2 + \frac{dz^2}{c_{\parallel}^2 - v^2(z)}. \quad (6)$$

By performing a coordinate transformation, $\tau = t + \int^z dz v(z)/[c_{\parallel}^2 - v^2(z)]$, we obtain an effective line element that shares the same form of the radial part of the Schwarzschild line element for gravitational black holes [44]. Similar to the Schwarzschild metric which has a singularity at the Schwarzschild radius corresponding to an event horizon, the above metric also has a horizon (z_h), where the dragging velocity is equal to the local ‘‘speed of light’’ for quasiparticles, $v(z_h) = \pm c_{\parallel}$. The corresponding ‘‘Newtonian gravitational field’’ at horizons is given by $E_g(z_h) = \frac{v(z_h)}{c_{\parallel}^2} \frac{dv}{dz} \Big|_{z_h}$. According to the fitted parameters of Eq. (4), assuming $v(z) > -c_{\parallel}$ [$v(z) < -c_{\parallel}$] in the region $z > z_h$ ($z < z_h$), an inhomogeneous $\text{Zn}_2\text{In}_2\text{S}_5$ system can be derived (see Fig. 4). Hence all quasiparticles in the upper region ($z > z_h$) move upward, and cannot cross the $z = z_h$ plane, which indicates that this plane is the black-hole horizon. Consequently, the inner observers living in the lower region ($z < z_h$) cannot obtain any information from the upper region ($z > z_h$) if they can only use the relativistic quasiparticles for communication.

A black hole can slowly radiate away its mass by emitting a thermal flux at the horizon, as pointed out by Hawking [45]. The analogous model presented above not only suggests a different route to simulating an event horizon, but also facilitates the realization of the Hawking radiation analog in dynamically inhomogeneous type-III Dirac semimetals. Although this model is static in equilibrium, the dissipation

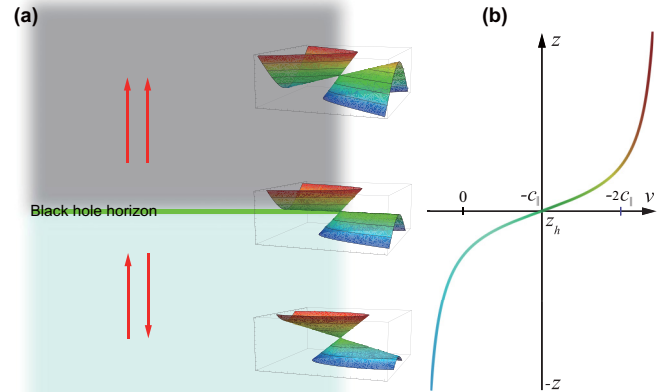


FIG. 4. (a) Schematic illustration of the solid-state analog of the black-hole horizon in an inhomogeneous $\text{Zn}_2\text{In}_2\text{S}_5$ with a controllable structural distortion. The red arrows indicate the quasiparticle propagating directions in each region. (b) The dependence of the dragging velocity v on the z coordinate.

process right after the creation of the black-hole-horizon analog is similar to the process of Hawking radiation [23–25]. The corresponding Hawking temperature can be determined by the ‘‘surface gravity’’ at the horizon $E_g(z_h)$ [37,43],

$$T_H = \frac{\hbar c_{\parallel}}{2\pi k_B} E_g(z_h) = \frac{\hbar}{2\pi k_B} \frac{dv}{dz} \Big|_{z_h}, \quad (7)$$

where k_B and \hbar are the Boltzmann and the reduced Planck constants, respectively. Obviously, T_H may reach a high temperature as long as the gradient of the dragging velocity is sufficiently large across the horizon. As the dragging velocity v is a material-dependent parameter which can be effectively tuned by strain and chemical doping [46,47], a high value of T_H is expected in inhomogeneous $\text{Zn}_2\text{In}_2\text{S}_5$.

Discussion. In conclusion, many recently emerging condensed matter analogs of high-energy particles are not real high-energy particles themselves, but quasiparticles of low-energy electronic excitations. But they have provided very interesting physics topics of study, which are of tremendous interest to both fields of condensed matter and particle physics. For the case we studied here, the causal structure of the type-III Dirac semimetal is identical to the causal structure of a black hole in the presence of fermions, although not the black hole itself. It is interesting to note that this analogy to a black hole by an electronic fluid is different from the ones made previously by a neutral fluid [35], because quantum effects are encoded already through density functional theory (DFT) calculations in the present case. So, some form of analogous ‘‘Hawking radiation’’ will definitely occur. In addition, other astrophysical phenomena such as a gravitational lensing effect [47], gravity wave [48], and a cosmological constant problem [36] can also be explored in type-III Dirac semimetals.

Acknowledgments. We thank Yong-Shi Wu and Jaakko Nissinen for helpful discussions. This work was supported by U.S. DOE-BES (Grant No. DE-FG02-04ER46148). The calculations were done on the CHPC at the University of Utah and DOE-NERSC.

- [1] D. J. Thouless, M. Kohmoto, M. P. Nightingale, and M. den Nijs, *Phys. Rev. Lett.* **49**, 405 (1982).
- [2] F. D. M. Haldane, *Phys. Rev. Lett.* **50**, 1153 (1983).
- [3] J. M. Kosterlitz and D. J. Thouless, *J. Phys. C* **5**, L124 (1972); **6**, 1181 (1973).
- [4] C. L. Kane and E. J. Mele, *Phys. Rev. Lett.* **95**, 146802 (2005); **95**, 226801 (2005).
- [5] B. A. Bernevig, T. L. Hughes, and S.-C. Zhang, *Science* **314**, 1757 (2006).
- [6] M. König, S. Wiedmann, C. Brüne, A. Roth, H. Buhmann, L. W. Molenkamp, X.-L. Qi, and S.-C. Zhang, *Science* **318**, 766 (2007).
- [7] L. Fu, *Phys. Rev. Lett.* **106**, 106802 (2011).
- [8] T. H. Hsieh, H. Lin, J. Liu, W. Duan, A. Bansil, and L. Fu, *Nat. Commun.* **3**, 982 (2012).
- [9] Y. Tanaka, Z. Ren, T. Sato, K. Nakayama, S. Souma, T. Takahashi, K. Segawa, and Y. Ando, *Nat. Phys.* **8**, 800 (2012); P. Dziawa, B. Kowalski, K. Dybko, R. Buczko, A. Szczerbakow, M. Szot, E. Łusakowska, T. Balasubramanian, B. M. Wojek, M. Berntsen *et al.*, *Nat. Mater.* **11**, 1023 (2012); Y. Okada, M. Serbyn, H. Lin, D. Walkup, W. Zhou, C. Dhital, M. Neupane, S. Xu, Y. J. Wang, R. Sankar *et al.*, *Science* **341**, 1496 (2013).
- [10] Z. Wang, Y. Sun, X.-Q. Chen, C. Franchini, G. Xu, H. Weng, X. Dai, and Z. Fang, *Phys. Rev. B* **85**, 195320 (2012).
- [11] Z. K. Liu, B. Zhou, Y. Zhang *et al.*, *Science* **343**, 864 (2014); S.-Y. Xu, C. Liu, S. K. Kushwaha *et al.*, *ibid.* **347**, 294 (2015).
- [12] Z. Wang, H. Weng, Q. Wu, X. Dai, and Z. Fang, *Phys. Rev. B* **88**, 125427 (2013).
- [13] M. Neupane, S.-Y. Xu, R. Sankar *et al.*, *Nat. Commun.* **5**, 3786 (2014); Z. K. Liu, J. Jiang, B. Zhou *et al.*, *Nat. Mater.* **13**, 677 (2014).
- [14] A. A. Burkov, M. D. Hook, and L. Balents, *Phys. Rev. B* **84**, 235126 (2011).
- [15] X. Wan, A. M. Turner, A. Vishwanath, and S. Y. Savrasov, *Phys. Rev. B* **83**, 205101 (2011).
- [16] H. Weng, C. Fang, Z. Fang, B. A. Bernevig, and X. Dai, *Phys. Rev. X* **5**, 011029 (2015); S.-M. Huang, S.-Y. Xu, I. Belopolski, C.-C. Lee, G. Chang, B. Wang, N. Alidoust, G. Bian, M. Neupane, C. Zhang *et al.*, *Nat. Commun.* **6**, 7373 (2015).
- [17] S.-Y. Xu, I. Belopolski, N. Alidoust, M. Neupane, G. Bian, C. Zhang, R. Sankar, G. Chang, Z. Yuan, C.-C. Lee *et al.*, *Science* **349**, 613 (2015); L. Yang, Z. Liu, Y. Sun, H. Peng, H. Yang, T. Zhang, B. Zhou, Y. Zhang, Y. Guo, M. Rahn *et al.*, *Nat. Phys.* **11**, 728 (2015); B. Lv, N. Xu, H. Weng, J. Ma, P. Richard, X. Huang, L. Zhao, G. Chen, C. Matt, F. Bisti *et al.*, *ibid.* **11**, 724 (2015).
- [18] A. A. Soluyanov, D. Gresch, Z. Wang, Q. Wu, M. Troyer, X. Dai, and B. A. Bernevig, *Nature (London)* **527**, 495 (2015).
- [19] K. Deng, G. Wan, P. Deng *et al.*, *Nat. Phys.* **12**, 1105 (2016).
- [20] H. Huang, S. Zhou, and W. Duan, *Phys. Rev. B* **94**, 121117 (2016).
- [21] M. Yan, H. Huang, K. Zhang, E. Wang, W. Yao, K. Deng, G. Wan, H. Zhang, M. Arita, H. Yang, Z. Sun, H. Yao, Y. Wu, S. Fan, W. Duan, and S. Zhou, *Nat. Commun.* **8**, 257 (2017).
- [22] T.-R. Chang, S.-Y. Xu, D. S. Sanchez, W.-F. Tsai, S.-M. Huang, G. Chang, C.-H. Hsu, G. Bian, I. Belopolski, Z.-M. Yu, S. A. Yang, T. Neupert, H.-T. Jeng, H. Lin, and M. Z. Hasan, *Phys. Rev. Lett.* **119**, 026404 (2017).
- [23] G. E. Volovik, *JETP Lett.* **104**, 645 (2016).
- [24] G. E. Volovik and K. Zhang, *J. Low Temp. Phys.* **189**, 276 (2017).
- [25] G. E. Volovik, *Phys.-Usp.* **61**, 89 (2018).
- [26] A. A. Abrikosov, *Phys. Rev. B* **58**, 2788 (1998).
- [27] C. Shekhar, A. K. Nayak, Y. Sun, M. Schmidt, M. Nicklas, I. Leermakers, U. Zeitler, Y. Skourski, J. Wosnitza, Z. Liu *et al.*, *Nat. Phys.* **11**, 645 (2015).
- [28] T. Liang, Q. Gibson, M. N. Ali, M. Liu, R. Cava, and N. Ong, *Nat. Mater.* **14**, 280 (2015).
- [29] H. B. Nielsen and M. Ninomiya, *Phys. Lett. B* **130**, 389 (1983).
- [30] Y. Wang, E. Liu, H. Liu, Y. Pan, L. Zhang, J. Zeng, Y. Fu, M. Wang, K. Xu, Z. Huang *et al.*, *Nat. Commun.* **7**, 13142 (2016).
- [31] J. Xiong, S. K. Kushwaha, T. Liang, J. W. Krizan, M. Hirschberger, W. Wang, R. Cava, and N. Ong, *Science* **350**, 413 (2015).
- [32] C.-Z. Li, L.-X. Wang, H. Liu, J. Wang, Z.-M. Liao, and D.-P. Yu, *Nat. Commun.* **6**, 10137 (2015); H. Li, H. He, H.-Z. Lu, H. Zhang, H. Liu, R. Ma, Z. Fan, S.-Q. Shen, and J. Wang, *ibid.* **7**, 10301 (2016).
- [33] C.-L. Zhang, S.-Y. Xu, I. Belopolski, Z. Yuan, Z. Lin, B. Tong, G. Bian, N. Alidoust, C.-C. Lee, S.-M. Huang *et al.*, *Nat. Commun.* **7**, 10735 (2016); X. Huang, L. Zhao, Y. Long, P. Wang, D. Chen, Z. Yang, H. Liang, M. Xue, H. Weng, Z. Fang, X. Dai, and G. Chen, *Phys. Rev. X* **5**, 031023 (2015).
- [34] H. Huang and F. Liu, *Phys. Rev. B* **95**, 201101 (2017).
- [35] W. G. Unruh, *Phys. Rev. Lett.* **46**, 1351 (1981); *Phys. Rev. D* **51**, 2827 (1995); M. Visser, *Class. Quantum Grav.* **15**, 1767 (1998).
- [36] T. A. Jacobson and G. E. Volovik, *Phys. Rev. D* **58**, 064021 (1998); G. E. Volovik, *Phys. Rep.* **351**, 195 (2001).
- [37] G. E. Volovik, *The Universe in a Helium Droplet*, Vol. 117 (Oxford University Press, Oxford, U.K., 2003).
- [38] L. J. Garay, J. R. Anglin, J. I. Cirac, and P. Zoller, *Phys. Rev. Lett.* **85**, 4643 (2000).
- [39] J. Steinhauer, *Nat. Phys.* **10**, 864 (2014); **12**, 959 (2016).
- [40] Z.-M. Yu, Y. Yao, and S. A. Yang, *Phys. Rev. Lett.* **117**, 077202 (2016); M. Udagawa and E. J. Bergholtz, *ibid.* **117**, 086401 (2016); S. Tchoumakov, M. Cividini, and M. O. Goerbig, *ibid.* **117**, 086402 (2016).
- [41] We note that the type-I and type-II Dirac/Weyl fermions in these semimetals can be further distinguished from the so-called type-III and type-IV ones with complex frequencies, as discussed in Ref. [49], which is different from the type-III fermions in this work.
- [42] See Supplemental Material at <http://link.aps.org/supplemental/10.1103/PhysRevB.98.121110>, for more details about the computation, which includes Refs. [4,20,23,24,40,46,50–55].
- [43] M. Novello, M. Visser, and G. E. Volovik, *Artificial Black Holes* (World Scientific, Singapore, 2002).
- [44] Ø. Grøn and S. Hervik, *Einstein's General Theory of Relativity: With Modern Applications in Cosmology* (Springer, New York, 2007).
- [45] S. W. Hawking, *Nature (London)* **248**, 30 (1974); *Commun. Math. Phys.* **43**, 199 (1975).
- [46] C. Le, S. Qin, X. Wu, X. Dai, P. Fu, C. Fang, and J. Hu, *Phys. Rev. B* **96**, 115121 (2017).
- [47] S. Guan, Z.-M. Yu, Y. Liu, G.-B. Liu, L. Dong, Y. Lu, Y. Yao, and S. A. Yang, *npj Quantum Mater.* **2**, 23 (2017).
- [48] R. Schützhold and W. G. Unruh, *Phys. Rev. D* **66**, 044019 (2002).

- [49] J. Nissinen and G. E. Volovik, *JETP Lett.* **105**, 447 (2017).
- [50] G. Kresse and J. Furthmüller, *Comput. Mater. Sci.* **6**, 15 (1996), <https://www.vasp.at/>.
- [51] J. P. Perdew, K. Burke, and M. Ernzerhof, *Phys. Rev. Lett.* **77**, 3865 (1996).
- [52] A. A. Mostofi, J. R. Yates, Y.-S. Lee, I. Souza, D. Vanderbilt, and N. Marzari, *Comput. Phys. Commun.* **178**, 685 (2008), <http://www.wannier.org/>.
- [53] M. P. López Sancho, J. M. López Sancho, and J. Rubio, *J. Phys. F* **14**, 1205 (1984); **15**, 851 (1985).
- [54] A. Jain, S. P. Ong, G. Hautier, W. Chen, W. D. Richards, S. Dacek, S. Cholia, D. Gunter, D. Skinner, G. Ceder, and K. A. Persson, *APL Mater.* **1**, 011002 (2013), <https://materialsproject.org/>.
- [55] A. A. Soluyanov and D. Vanderbilt, *Phys. Rev. B* **83**, 235401 (2011).